1646 *Journal of Mechanical Science and Technology (KSME Int. J.), Vol. 20, No. 10, pp. 1646~1652, 2006*

Modeling of Mechanical Behavior of Microcantilever due to Intrinsic Strain during Deposition

Sang-Hyun Kim*
CSE Center, Samsung Advanced Institute of Technology,
Mt. 14-1, Nongseo-dong, Giheung-gu, Younggin-si, Gyunggi-do 449-712, Korea
Sathyanarayanan Mani, James G. Boyd IV
Department of Aerospace Engineering,
3141 TAMU, Texas A&M University, College Station, TX, 77843-3141, USA

A model of mechanical behavior of microcantilever due to intrinsic strain during deposition of MEMS structures is derived. A linear ordinary differential equation is derived for the beam deflection as a function of the thickness of the deposited layer. Closed-form solutions are not possible, but numerical solutions are plotted for various dimensionless ratios of the beam stiffness, the intrinsic strain, and the elastic moduli of the substrate and deposited layer. This model predicts the deflection of the cantilever as a function of the deposited layer thickness and the residual stress distribution during deposition. The usefulness of these equations is that they are indicative of the real time behavior of the structures, i.e. it predicts the deflection of the beam continuously during deposition process.

Key Words : Multilayer Microcantilever, Residual Stress, Deposition, Intrinsic Strain, Beam Deflection

1. Introduction

Micromachined multilayer cantilevers have been widely used in microelectronics, optical and structural components (Wu et al., 1995 ; Tien et al., 1996 ; Kiang et al., 1996). The mechanical response of multilayer cantilevers is affected by residual stresses, which are generated from the fabrication process such as physical or chemical vapor deposition, sputtering and electroplating. Due to the mismatch between the deposited film and the substrate, a residual stress is generated, which subsequently causes a deformation in the cantilever. For instance, a residual bending moment will warp released structures such as cantilevers (Mitchell and Hanson, 2002), as shown in Fig. 1. Thus, residual stresses usually have deleterious effects in thin film processing, such as film buckling, warping, blistering, cracking, delamination and void formation. Recently, out-of-plane microcantilevers under initial bending have been usefully integrated in many applications, such as microelastic joints (Yasuda, 1995), micro-scanners (Schweizer et al., 1999) and microwave switches (Chang and Chang, 2000).

In order not to use the trials and errors it is desirable to be able to predict the final shape of multilayer microcantilevers due to the residual stresses, especially the intrinsic stress. Attention has been devoted recently to the analysis of multilayer structure under thermal and intrinsic stress. Hsueh (2002), and Hu and Huang (2004) derived simple approaches for the closed form solution in multilayer thin film structure under thermal influences. Nikishkov (2003) and Nikishkov et al. (2003) derived the analytical solution and

* Corresponding Author,
E-mail : shkim004@gmail.com
TEL : +82-31-280-8146; **FAX** : +82-31-280-9158
CSE Center, Samsung Advanced Institute of Technology, Mt. 14-1, Nongseo-dong, Giheung-gu, Younggin-si, Gyunggi-do 449-712, Korea. (Manuscript **Received** February 13, 2006; **Revised** July 9, 2006)

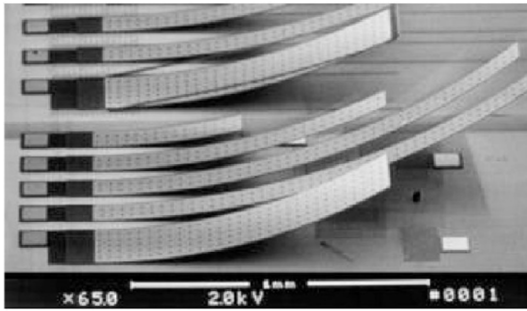

Fig. 1 SEM photography of cantilevers with significant stress-induced bending

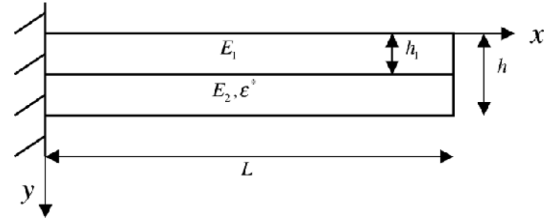

Fig. 2 Schematic of the microcantilever

numerical modeling suitable for hinged multilayer structure. They accounted for the initial strain due to the lattice mismatch or thermal loading. However, it is not suitable to predict the real time behavior of the structure during deposition process.

This research presents a model of mechanical behavior of microcantilever due to intrinsic strain during deposition of MEMS structures. In order to develop this model the behavior of thin film structures under the influences of residual stresses has been understood and analyzed. This model predicts the deflection of the cantilever as a function of the thickness of the deposited layer and the residual stress distribution during deposition. The usefulness of these equations is that they are indicative of the real time behavior of the structures, i.e. it predicts the deflection of the beam continuously during deposition process.

2. Theoretical Modeling

2.1 Problem formulation and assumption

Consider a case where in a material that is different from the substrate is deposited on the cantilever substrate as shown in Fig. 2. Due to the mismatch between the deposited film and the substrate, a residual stress is generated, which subsequently causes a deformation in the cantilever. The prismatic beam has constant length L, constant width b, and variable thickness h. The substrate with Young's modulus of E_1 is designated as region 1 and has a constant thickness h_1. The deposited material with Young's modulus of E_2 has a variable thickness h_2, and $h=h_1+h_2$. Material is then deposited on the surface $y=h(h\geq h_1)$, which causes the beam to bend either up or down, depending on the sign of the mismatch strain in the deposited material. The goal of the present derivation is to obtain an equation for the beam deflection as a function of h during deposition.

The input to the problem is the increment of thickness, dh, i.e. all changes in the configuration are due only to a changing h. There is no time dependence, so all rates can be replaced by increments. For example, the increment of bending stress $d\sigma$ can be used instead of the time derivative $d\sigma/dt$. Brackets are used to denote the functional dependence of variables. For example, the bending stress $\sigma\{x,y;h\}$ is a function of x and y as well as the thickness h. The bending stress and elastic strain $\varepsilon^e\{x,y;h\}$ are related by Hooke's law,

$$\sigma\{x,y;h\}=E\{y\}\varepsilon^e\{x,y;h\} \tag{1}$$

where the Young's modulus is given by

$$E\{y\}=\begin{cases}E_1, & 0\leq y\leq h_1\\ E_2, & h_1<y\leq h\end{cases}$$

The elastic strain is the sum of the total strain $\varepsilon\{x,y;h\}$ and the mismatch strain $\varepsilon^m\{x,y\}$

$$\varepsilon^e\{x,y;h\}=\varepsilon\{x,y;h\}+\varepsilon^m\{x,y\} \tag{2}$$

where the mismatch strain is due to growth processes or lattice mismatch between the deposited material and the deposited surface. The total strain satisfies the compatibility equations, i.e. it can be derived by taking the derivatives of a continuous and single-valued displacement field. In general, neither the elastic strain nor the mismatch strain can be obtained from continuous displacement fields. The total strain obeys the

Kirchhoff kinematic assumptions of Euler-Bernoulli beam theory,

$$\varepsilon\{x,y;h\}=-y\kappa\{x;h\}+\varepsilon^r\{x;h\} \tag{3}$$

where $\kappa\{x;h\}$ is the curvature about the z axis and $\varepsilon^r\{x;h\}$ is the strain of the reference layer, $y=0$. The increment of total strain is given by

$$d\varepsilon\{x,y;h\}=-yd\kappa\{x;h\}+d\varepsilon^r\{x;h\} \tag{4}$$

The reference value ε^* of the mismatch strain is the mismatch strain that results from deposition on a strain-free substrate; for example, a flat substrate that is free of stress. ε^* is constant, so $d\varepsilon^*=0$. As material is deposited with non-zero mismatch strain, both the substrate and the deposited layer will bend. Thus, material will be deposited on a strained surface with non-zero curvature. This bending strain $\varepsilon^d\{x,y\}$ on the deposition surface must be subtracted from ε^* to obtain the total mismatch strain,

$$\varepsilon^m\{x,y\}=\varepsilon^*-\varepsilon^d\{x,y\} \tag{5}$$

The strain $\varepsilon^d\{x,y\}$ is the value of $\varepsilon\{x,y;h\}$ evaluated on the deposition surface, $y=h$, at the time that the material was deposited. Thus, the value of $\varepsilon^d\{x,y\}$ at any point y is equal to $\varepsilon\{x,y;h\}$ evaluated at $h=y$:

$$\varepsilon^d\{x,y\}=-y\kappa\{x;y\}+\varepsilon^r\{x;y\} \tag{6}$$

The most useful form of the mismatch strain is obtained by substituting Eq. (6) into Eq. (5):

$$\begin{aligned}\varepsilon^m\{x,y\}&=\varepsilon^*-\varepsilon^d\{x,y\}\\&=\varepsilon^*+y\kappa\{x;y\}-\varepsilon^r\{x;y\}\end{aligned} \tag{7}$$

Although the strain $\varepsilon\{x,y;h\}$ at a given point (x,y) changes as $\kappa\{x;y\}$ changes with h, the strain $\varepsilon^d\{x,y\}$ is not a function of h, and $d\varepsilon^d\{x,y\}=0$. The mismatch strain $\varepsilon^m\{x,y\}$ is also constant with respect to h, and $d\varepsilon^m\{x,y\}=0$, and it follows from Eq. (2) that

$$d\varepsilon^e\{x,y;h\}=d\varepsilon\{x,y;h\} \tag{8}$$

The elastic strain on the deposition surface is obtained by substituting Eqs. (7) and (3) into Eq. (2) and evaluating at $y=h$ to obtain

$$\varepsilon^e\{x,h;h\}=\varepsilon^* \tag{9}$$

2.2 Generalized differential equation formulation

In order to get a relation between the deflection and the deposit thickness two equilibrium conditions, the moment equilibrium and the horizontal force equilibrium are considered to formulate a numerically solvable differential equation. The equilibrium equations for the moment about the z axis and the horizontal force in the x direction provide two equations for the two increments $d\kappa\{x;h\}$ and $d\varepsilon^r\{x;h\}$
The moment equilibrium is given by:

$$\begin{aligned}dM\{x;h\}=b\int_0^h d\sigma\{x,y;h\}ydy\\+bh\sigma\{x,y;h\}dh\end{aligned} \tag{10}$$

where $M\{x;h_1\}$. The stress increment is obtained by substituting Eq. (8) into Eq. (1):

$$d\sigma\{x,y;h\}=\begin{cases}E_1 d\varepsilon\{x,y;h\}, & 0\le y\le h_1\\ E_2 d\varepsilon\{x,y;h\}, & h_1<y\le h\end{cases} \tag{11}$$

The stress on the deposition surface is obtained by substituting Eq. (9) into Eq. (1):

$$\sigma\{x,h;h\}=E_2\varepsilon^e\{x,h;h\}=E_2\varepsilon^* \tag{12}$$

Substitution of Eqs. (11), (12) and (4) into Eq. (10) yields the moment increment

$$\begin{aligned}dM\{x;h\}=&\left(-\frac{1}{3}bE_2h^3-\frac{1}{3}bh_1^3(E_1-E_2)\right)d\kappa\{x;h\}\\&+bE_2\varepsilon^*hdh\\&+\left(\frac{1}{2}bE_2h^2+\frac{1}{2}bh_1^2(E_1-E_2)\right)d\varepsilon^r\{x;h\}\end{aligned} \tag{13}$$

A similar procedure for the horizontal force equilibrium yields

$$\begin{aligned}0&=b\int_0^h d\sigma\{x,h;h\}dy+b\sigma\{x,h;h\}dh\\&=b\int_0^h E\{y\}(-yd\kappa\{x;h\}+d\varepsilon^r\{x;h\})dy+bE_2\varepsilon^*dh\\&=\left(-\frac{1}{2}E_2h^2-\frac{1}{2}(E_1-E_2)h_1^2\right)d\kappa\{x;h\}\\&\quad+E_2\varepsilon^*dh+(E_2hd+(E_1-E_2)h_1)d\varepsilon^r\{x;h\}\end{aligned} \tag{14}$$

$d\varepsilon^r\{x;h\}$ can be eliminated from Eqs. (13) and (14) to obtain the moment increment in terms of

the curvature increment and the thickness increment:

$$\frac{dM\{x;h\}}{bE_1}=\frac{1}{12\bar{E}}f\{h\}d\kappa\{x;h\}+\frac{\varepsilon^*}{2\bar{E}}g\{h\}dh \tag{15}$$

where $\bar{E}=E_1/E_2$ and

$$f\{h\}=(h+(\bar{E}-1)h_1)^{-1}(-h^4-4h^3h_1(\bar{E}-1)+6h^2h_1^2(\bar{E}-1)-4hh_1^3(\bar{E}-1)-h_1^4(\bar{E}-1)^2)$$

$$g\{h\}=(h+(\bar{E}-1)h_1)^{-1}(h^2+2hh_1(\bar{E}-1)-h_1^2(\bar{E}-1))$$

To derive the beam deflection it is necessary to introduce the approximate increment of curvature as

$$d\kappa\{x;h\}=\frac{d^2}{dx^2}dv\{x;h\} \tag{16}$$

where $v\{x;h\}$ is the displacement of the beam in the y direction. Since zero moment about the z axis, Eq. (16) can be substituted into Eq. (15) to yield

$$\frac{d^2}{dx^2}dv\{x;h\}=-6\varepsilon^*\frac{g\{h\}}{f\{h\}}dh \tag{17}$$

Integrating Eq. (17) twice with respect to x results in

$$dv\{x;h\}=-3\varepsilon^*\frac{g\{h\}}{f\{h\}}dhx^2+c_1x+c_2 \tag{18}$$

The boundary conditions $0=v\{0;h\}=d/dx\, v\{0;h\}$ yield $0=c_1=c_2$, so that Eq. (18) at the end of cantilever becomes

$$\frac{dv\{L;h\}}{dh}=-3\varepsilon^*\frac{g\{h\}}{f\{h\}}L^2 \tag{19}$$

The non-dimensional form of Eq. (19) is given by

$$\frac{d\bar{v}\{\bar{h}\}}{d\bar{h}}=-3s\frac{\bar{g}\{\bar{h}\}}{\bar{f}\{\bar{h}\}} \tag{20}$$

where,

$\bar{h}=h/h_1$, $\bar{L}=L/h_1$, $\bar{v}\{\bar{h}\}=v\{L,\bar{h}\}/h_1$, $s=\varepsilon^*\bar{L}^2$,

$$\bar{f}\{\bar{h}\}=(\bar{h}+(\bar{E}-1))^{-1}(-\bar{h}^4-4\bar{h}^3(\bar{E}-1)+6\bar{h}^2(\bar{E}-1)-4\bar{h}(\bar{E}-1)-(\bar{E}-1)^2),$$ and

$$\bar{g}\{\bar{h}\}=(\bar{h}+(\bar{E}-1))^{-1}(\bar{h}^2+2\bar{h}(\bar{E}-1)-(\bar{E}-1)).$$

Eq. (20) is an ordinary linear differential equation for the non-dimensional end-deflection $\bar{v}\{\bar{h}\}$ as a function of the non-dimensional thickness $\bar{h}$. Unfortunately, Eq. (20) must be numerically integrated. Fig. 3 shows the numerically solved beam deflection during deposition for various values of the non-dimensional parameters s. The ratio $\bar{E}$ of Young's moduli is 168/200, which corresponds to a silicon substrate and a deposited layer of Permalloy (Ni/Fe alloy). For a given ratio of Young's moduli, the deflection increases with increasing s (i.e. a larger mismatch strain or a longer beam). The rate of deflection with the deposited thickness is decreasing, which indicates the influence of the intrinsic strain is decreasing

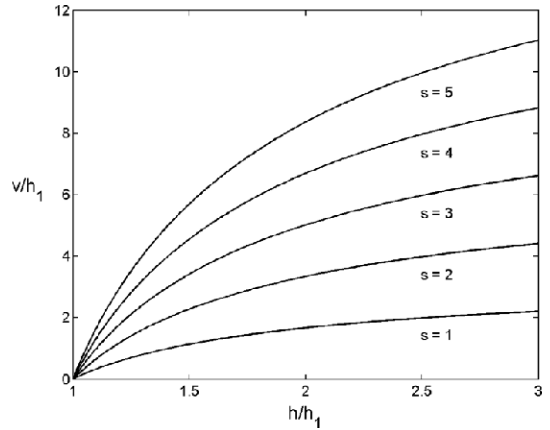

Fig. 3 Deflection during deposition for various values of the non-dimensional parameters s

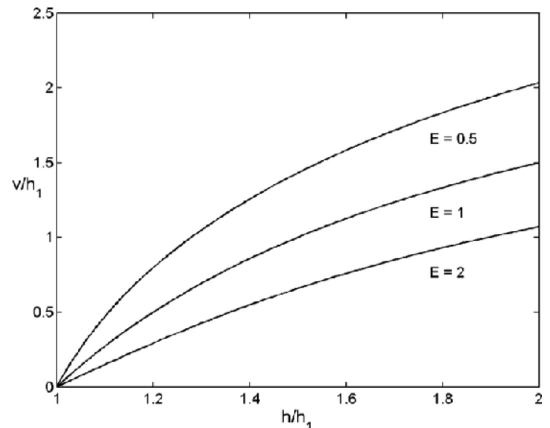

Fig. 4 Deflection during deposition for various values of the Young's moduli

as increasing the deposited thickness. Fig. 4 gives the relation between the beam deflection and the ratio of Young's moduli for a given non-dimensional parameters s. As expected, the more compliant substrate (smaller $\bar{E}$) results in a greater deflection.

3. Stress Distribution

It is extremely important to know about the stress distribution in the cantilever because it gives an idea where the stresses are maximum. It also tells which areas are critical and present potential failure spots. To calculate the stress distribution it is required to integrate the incremental stress created due to the deposition of each layer.

The incremental stress due to deposition is given by Eq. (11). Using Eq. (4), Eq. (11) can be rewritten as:

$$d\sigma\{x,y;h\} = \begin{cases} E_1(-yd\kappa\{x;y\}+d\varepsilon^r\{x;y\}), & 0\le y\le h_1 \\ E_2(-yd\kappa\{x;y\}+d\varepsilon^r\{x;y\}), & h_1<y\le h \end{cases} \quad (21)$$

The incremental reference strain is given by using Eq. (14) :

$$d\varepsilon^r\{x;h\}=\frac{\left(\frac{h^2}{2}+\frac{\bar{E}-1}{2}h_1^2\right)d\kappa\{x;h\}-\varepsilon^* dh}{h+(\bar{E}-1)h_1} \quad (22)$$

Setting $dM\{x;h\}=0$ in Eq. (15) yields:

$$d\kappa\{x;h\}=-6\varepsilon^*\frac{g\{h\}}{f\{h\}}dh \quad (23)$$

Using Eqs. (22) and (23), Eq. (21) can be rewritten as:

$$d\sigma\{x,y;h\}=\begin{cases} E_1N\{h\}, & 0\le y\le h_1 \\ E_2N\{h\}, & h_1<y\le h \end{cases} \quad (24)$$

where,

$$N\{h\}=\left\{6\varepsilon^* y\frac{g\{h\}}{f\{h\}} + (h+(\bar{E}-1)h_1)^{-1}\left[\left(\frac{h^2}{2}+\frac{\bar{E}-1}{2}h_1^2\right)\left(-6\varepsilon^*\frac{g\{h\}}{h\{h\}}\right)-\varepsilon^*\right]\right\}dh$$

Consider the case of material with the same Young's modulus as the substrate ($\bar{E}=1$). In this case, $f\{h\}=-h^3$, $g\{h\}=h$, and Eq. (24) yields the incremental stress distribution in case of the homogeneous deposition:

$$d\sigma\{x,y;h\}=E_1\left(-6\varepsilon^*\frac{y}{h^2}+2\varepsilon^*\frac{1}{h}\right)dh \quad (25)$$

Integrating Eq. (25) with respect to h and using the boundary condition,

$$\sigma\{x,y;h_1\}=0$$

gives the stress distribution in the cantilever for homogeneous deposition:

$$\sigma\{x,y;h\}=2E_1\varepsilon^*\left(\ln\frac{h}{h_1}-\frac{3y}{h_1}\left(1-\frac{h_1}{h}\right)\right), \quad h_1<y\le h \quad (26)$$

Eq. (26) can be rewritten as:

$$\sigma\{x,\bar{y};\bar{h}\}=2\sigma_1\left(\ln\bar{h}-3\bar{y}\left(1-\frac{1}{\bar{h}}\right)\right), \quad 1<\bar{y}\le\bar{h} \quad (27)$$

where, $\sigma_1=E_1\varepsilon^*$

Figure 5 presents the normalized stress distribution along the non-dimensionalized depth of the cantilever as a function of the non-dimensionalized deposit thickness. Fig. 6 clearly depicts the stress distribution's dependence on the non-dimensionalized deposit thickness and the Fig. 7 shows the variation of the stress along the depth of the cantilever beam for various deposit thickness. It is seen that for small deposit thickness the stress distribution is almost linear.

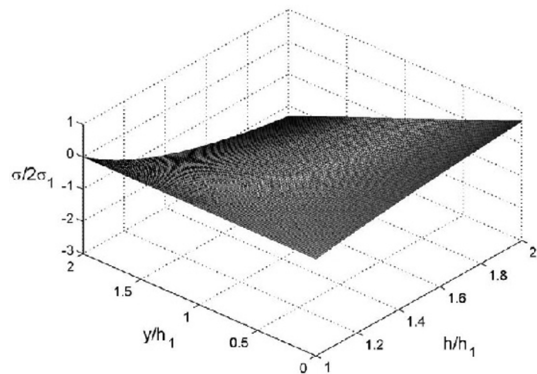

Fig. 5 A 3D representation of the residual stress in the cantilever

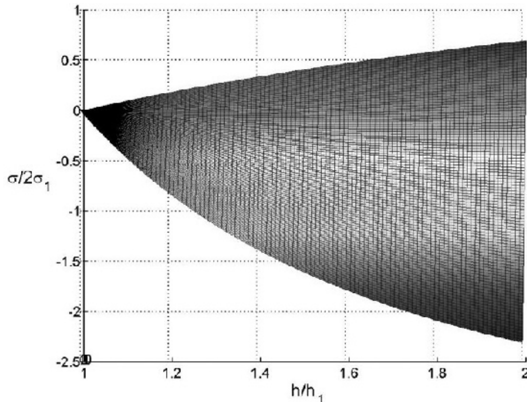

Fig. 6 Residual stress plot as a function of h/h_1

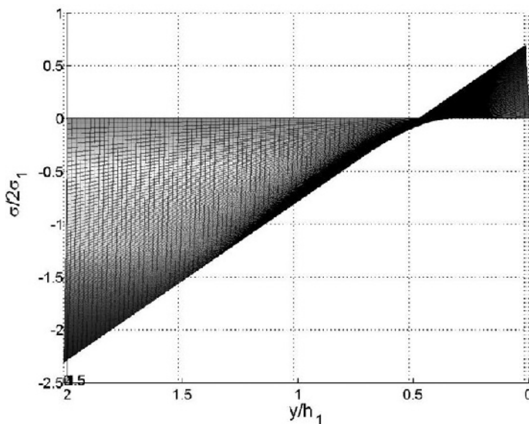

Fig. 7 Residual stress plot as a function of y/h_1

4. Conclusions

This research presents a model of mechanical behavior of microcantilever due to intrinsic strain during deposition of MEMS structures. In order to develop this model the behavior of thin film structures under the influences of residual stresses has been understood and analyzed. This model predicts the deflection of the cantilever as a function of the thickness of the deposited layer and the residual stress distribution during deposition. The usefulness of these equations is that they are indicative of the real time behavior of the structures, i.e. it predicts the deflection of the beam continuously during deposition process. The results of the theoretical analyses are listed below :

(1) For a given ratio of Young's moduli, the deflection increases with increasing (i.e. a larger mismatch strain or longer beam). The more compliant substrate (smaller $\bar{E}$) results in a greater deflection.

(2) The stress distribution plots indicate that the stress distribution is almost linear along the depth of the cantilever. If the mismatch strain is positive then the beam is predominantly under compression and vice-versa. That is to say that a tensile deposit will bend the substrate concave and a compressive stress would bend it convex.

(3) For more accurate prediction of the intrinsic strain induced beam deflection during deposition process, the reference mismatch strain should be measured by experiment.

References

Chang, C. and Chang, P., 2000, "Innovative Micromachined Microswitch with Very Low Insertion Loss," *Sensors and Actuators*, Vol. A79, pp. 71～75.

Hsueh, C. -H., 2002, "Modeling of Elastic Deformation of Multilayers Due to Residual Stresses and External Bending," *Journal of Applied Physics*, Vol. 91, pp. 9652～9656.

Hu, Y. Y. and Huang, W. M., 2004, "Elastic and Elastic-Plastic Analysis of Multilayer Thin Films : Closed-Form Solutions," *Journal of Applied Physics*, Vol. 96, pp. 4154～4160.

Kiang, M. H., Solgaard, O., Muller, R. S. and Lau, K. Y., 1996, "Silicon-Micromachined Micromirrors with Integral High-Precision Actuators for External-Cavity Semiconductor Laser," *IEEE* Photonics Technology Letters, Vol. 8, pp. 95～97.

Madou, M., 1993, *Fundamentals of Microfabrication*, Boca Raton : CRC Press, LLC.

Mitchell, J. N. and Hanson, H. S., 2002, "Investigation of Micro Electromechanical Systems -Fabricated Actuators for Use in Optical and Mechanical Applications," www.swri.edu, IR&D Report, Accessed in October.

Nikishkov, G. P., 2003, "Curvature Estimation for Multilayer Hinged Structures with Initial Strains," *Journal of Applied Physics*, Vol. 94, pp. 5333～5336.

Nikishkov, G. P., Khmyrova, I. and Ryzhil, V.,

2003, "Finite Element Analysis of Self-Positioning Microstructures and Nanostructures," *Nanotehnology*, Vol. 14, pp. 820～823.

Schweizer, S., Calmes, S., Laudon, M. and Renaud, Ph., 1999, "Thermally Actuated Optical Microscanner with Large Angel and Low Consumption," *Sensors and Actuators*, Vol. A76, pp. 470～477.

Tien, N. C., Solgaard, O., Kiang, M.-H., Daneman, M., Lau, K. Y. and Muller, R. S., 1996, "Surface-Micromachined Mirrors for Laser-Beam Positioning," *Sensors and Actuators*, Vol. A52, pp. 76～80.

Wu, M. C., Lin, L.-Y. Lee, Lin, S.-S. and Pistor, S. J., 1995, "Micromachined Free-Space Integrate Micro-Optics," *Sensors and Actuators*, Vol. A50, pp. 127～134.

Yasuda, T., Shimoyama, I. and Miura, H., 1995, "Electrostatically Driven Micro Elastic Joints," *Proc. IEEE MEMS (MEMS'95)*, pp. 242～245.